Analytical Calculation and Experimental Validation of Litz Wires Axial Thermal Conductivity

Zhaozong Li, Zeyuan Xu, *Member, IEEE*, Fengyu Zhang, *Member, IEEE*, David Gerada, *Senior Member, IEEE*, Rong Guo, Hengliang Zhang, Martin Corfield, Chris Gerada, *Senior Member, IEEE*, and Chengning Zhang

***Abstract*—Litz wires are widely used in electrical machines with reduced AC losses, compared to traditional random winding. The reduced AC losses can improve both electrical machines electromagnetic performance, such as efficiency and thermal performance. Thermal aspect is identified as a key enabler for next generation high power density electrical machines, where thermal modelling plays a critical role. Equivalent slot thermal conductivity is one of the most challenging parameters to be determined in the process of thermal model development, due to various components, such as copper, insulation, and impregnation resin. There are extensive literatures where the litz wire thermal conductivity in the radial direction are reported. However, the thermal conductivity in the axial direction is not well studied, which is critical to determine the heat transfer, such as for electrical machines with end winding spray-cooling system. In this paper, the axial thermal conductivity is investigated with analytical calculations and experimental validation. Firstly, 9 litz wire samples are selected with various types, such as rectangular and circular shapes, with varnish process and without. Two different analytical methods are then introduced and presented to calculate the litz wire thermal conductivity in axial direction, based on equivalent length theory and equivalent medium theory, respectively. Finally, experimental tests are conducted, and results are compared to those obtained from the proposed analytical methods. Guidelines are also provided to predict the litz wire axial thermal conductivity in this field.**

***Index Terms*—Litz Wire, Thermal Conductivity, Equivalent Medium Theory, Axial Direction**

Manuscript received November 06 2022; revised February 02 2023; accepted March 12 2023.

Zhaozong Li is with the Power Electronics machines and Control group, University of Nottingham, Nottingham, NG7 2RD, UK and also with the National Engineering Research Center of Electric Vehicles in Beijing Institute of Technology, Beijing, 10081, China. (e-mail: zz_li312018@163.com)

Zeyuan Xu, Fengyu Zhang, David Gerada, Martin Corfield and Chris Gerada are with the Power Electronics, Machines and Control Group, University of Nottingham, Nottingham, NG7 2RD, UK. (e-mail: zeyuan.xu@nottingham.ac.uk; fengyu.zhang1@nottingham.ac.uk; david.gerada@nottingham.ac.uk; ezamc17@exmail.nottingham.ac.uk; chris.gerada@nottingham.ac.uk)

Rong Guo is with Beijing University of Civil Engineering and Architecture (e-mail: guorong@bucea.edu.cn)

Hengliang Zhang are with Southeast University, Nanjing, China (e-mail: zhanghengliang@seu.edu.cn)

Chengning Zhang is with the National Engineering Research Center of Electric Vehicles in Beijing Institute of Technology, Beijing, 10081, China. (e-mail: mrzhchn@bit.edu.cn).

I. INTRODUCTION

With the increasing demands in power electronic system performance, the design strategies are moving toward higher power density. Meanwhile, the high frequency technology has become more important in electric motors, transformers, and other equipment [1-3]. However, the higher AC losses due to the skin and proximity effects are problematic for high frequency electrical machines, which results into lower efficiency for the electromagnetic aspect and higher winding temperature for the thermal aspect. The application of litz wires with transposition features can effectively reduce this effect, which are widely used in high-performance motors [7-10]. Fig. 1 shows a litz wire electrical machine [7].

Fig. 1. Litz wire wound machine.

For electrical machines, in particular high performance electrical machines, thermal management is critical, where accurate thermal model is essential tool [5]. The thermal conductivity including the equivalent slot thermal conductivity is critical in the thermal model building up process. However, most existing literature focus on the thermal conductivity calculation in the radial direction, i.e., xy direction in Fig.2 [5-8], which is important for cooling technique such as water jacket cooling. However, there is much less research focused on the axial thermal conductivity, i.e., z direction in Fig.2. The axial thermal conductivity is important to build up the 3D model in the cooling system, where most of the heat is removed axially in winding, such as the end winding oil sprayed stator [11], and axial flux motor [13]. The methodology used to calculate the radial thermal conductivity [5] cannot be applied to the axial thermal conductivity calculation, in particular for litz wires. This is due to the fact

that litz wire has unique twisted structure with wrapped insulating material. The anisotropy heat transfer characteristic is more pronounced compared to that of traditional windings. This paper will focus on litz wires thermal conductivity determination in the axial direction, with two proposed analytical methods.

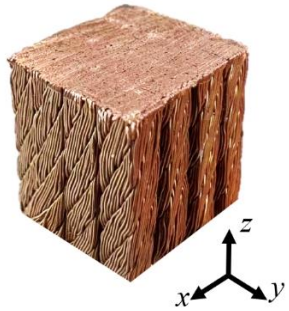

Fig. 2. Defining the direction of Litz wires

Generally, there are two main methods to estimate the coils thermal behavior for thermal conductivity calculation: finite element (FE) and analytical calculations. The FE analysis is the most widely used method at present [8, 14-19]. Compared to analytical calculations, it can provide more accurate results if the coils can be properly modelled. The effects of transposition and parallel arrangement on the litz wires thermal conductivity with FE model are discussed in [14]. FE is also used to simulate the equivalent model of winding and impregnation resin materials [16]. However, for much more complicated coil made of multi-layer litz, FE method may not be suitable due to the numerous time to build and calculate.

Analytical methods provide quicker solutions compared to FE. An equivalent model of a 3D porous cube was proposed in [7] to calculate litz wires thermal conductivity in the radial direction, which was validated with experimental results. Similarly, four 2D rectangular equivalent models on litz wire in the radial direction are proposed and compared in [9]. Analytical methods are quicker compared to FE model. In this paper, two analytical methods to consider litz wires complex features are proposed to calculate the equivalent axial thermal conductivity of litz wires. The novelties within the papers are:

- The complex structure of the litz wire, such as bundle distribution is considered within the two analytical calculations.
- The two analytical methods are proposed and compared for litz wires with various dimensions, validated with experimental results.
- Empirical formulas are proposed, and guidelines are presented to use the analytical methods.

The paper structure is as follows: section II presents the structure of various litz wire samples used for this study. Analytical calculation methodologies are introduced in section III, including the equivalent length model and equivalent medium model. Axial thermal conductivities of 9 litz wire samples are experimentally measured and compared with the analytical results proposed in section IV. Finally, section V concludes this paper.

II. Studied Objects

This section presents up to 9 litz wire samples used in this paper, shown in Fig.3, ordered from '$^{\#}a$' to '$^{\#}i$'. The physical structure of litz wire sample is briefly described firstly, and the main parameters of these samples are listed in TABLE I. More structure analysis discussions are followed in order to build up the theoretical models to estimate the equivalent axial thermal conductivities for various litz wires.

Fig. 3. Litz wire samples

A. Parameters of the Samples

In TABLE I, ***Shape*** is litz wires appearance, such as rectangular or circular. ***Cross-section***, A_e, and α are the litz wires cross-sectional profile, i.e., single wire cross-sectional area, and bundle twist angle, respectively. It should be noted that the bundle twist angle is the same as the wire twist angle inside each single bundle at the opposite direction if the litz wire is made of multi-layer bundles. Therefore, for litz wire you can see at the out layer of enameled wires are aligned with the cable direction, as shown in Fig.4.

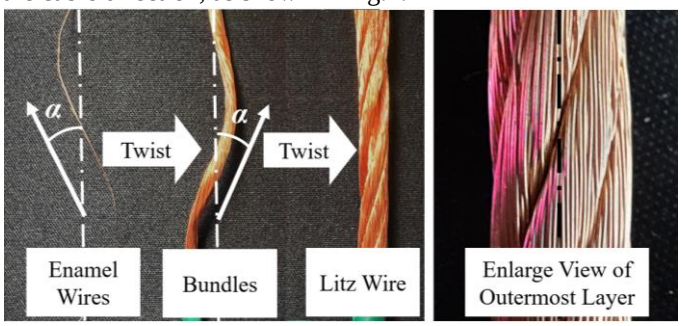

Fig. 4. Instruction of the twist angle α

Structure consists the litz wire major parameters of construction, including the number of litz wire layers N_l. There are three types of layer numbers in the studied objects, single-layer litz wire, double-layer litz wire, and triple-layer litz wire. Single-layer litz wire is directly twisted with u enameled wires, double-layer litz wire is twisted again with using v single-layer litz wires as its basic bundles, and triple-layer litz wire is using w double-layer litz wires as its sub-bundles to build, as shown in Fig.5.

TABLE I
SAMPLES PARAMETERS

Sample	*Shape*			*Structure*						*Material*		
	Cross-section	A_e	α	N_l	u	v	w	N_w	D_w	*Enamel Wires*	*Wrap*	*Varnish*
#*a*	Rectangle	3.0×3.8	22°	2	29	7	-	203	0.2	Cu(R)TD1	Nylon	Epoxylite
#*b*	Rectangle	3.2×3.4	12°	2	8	5	-	40	0.4	Cu(R)SH1	Nomex	-
#*c*	Rectangle	3.6×4.0	22°	2	12	6	-	72	0.4	Cu(R)TD1	Kapton	-
#*d*	Rectangle	4.6×3.6	16°	1	5	--	-	5	1.8	Cu(R)TD1	-	Epoxylite
#*e*	Rectangle	5.6×4.6	20°	3	10	6	7	420	0.2	Cu(R)TD1	-	Epoxylite
#*f*	Rectangle	6.8×6.0	18°	2	56	12	-	672	0.2	Cu(R)HP1	-	Epoxylite
#*g*	Rectangle	6.6×6.0	16°	2	17	10	-	170	0.4	Cu(R)TD1	-	Epoxylite
#*h*	Cylindrical	$3.3^2\pi$	16°	2	98	7	-	686	0.2	Cu(R)TD1	Kapton	-
#*i*	Cylindrical	$4.8^2\pi$	18°	2	35	10	-	350	0.4	Cu(R)HP1	Kapton	-

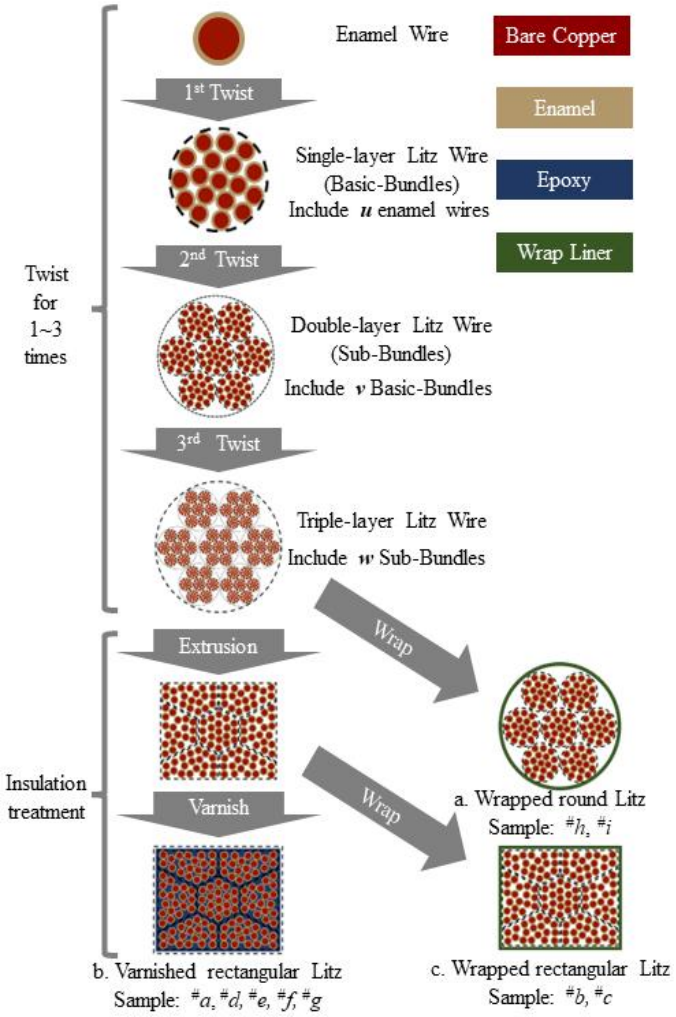

Fig. 5. Manufacture process of the litz wires

N_w is the total number of enameled wires in a litz wire. D_w is the bare copper diameter of each enameled wire. ***Material*** includes ***Enamel Wires***, ***Wrap***, and ***Varnish***, which represents the insulation material in the litz wire, and their thermal properties are listed in TABLE II using standard NFC 31010. The twisting process of 2-layer litz wires is detailed in Fig.5. As we can see, single wires are firstly twisted to form a basic bundle, which are furtherly twisted as sub-bundles and then can be twisted again to form a litz wire finally. The twisting times are depending on the layers of litz wire. Further compression or extrusion can be done if a rectangular cross-section litz wire is required.

TABLE II
THERMAL CONDUCTIVITY OF MATERIALS

Symbol	*Introduction*	*Thermal Conductive*
Cu (R)	Bare Copper	401 W / m·K
Cu 101	Copper [HC101]	391 W / m·K
Al 30TF	Aluminum [HE30TF]	180 W / m·K
TD	Enamel	≈0.81 W / m·K
HP	Enamel	≈0.81 W / m·K
SH	Enamel	≈1.21 W / m·K
Varnish	Epoxylite 235SG	≈0.26 W / m·K
Air	Under 20℃	0.024 W / m·K

The litz wire can be wrapped to get better insulation or varnished to keep the coil in shape. Among the 9 samples, samples #*b*, #*c*, #*h*, and #*i* are wrapped without varnish, and samples #*a*, #*d*, #*e*, #*g* are investigated for both conditions with varnish and without.

B. Bundles Distribution

The internal structure of litz wires is furtherly clarified in this section. There are 5, 6, 7, 10, and 12 bundles for the litz wires in Fig.3. The litz wires are twisted based on the internal middle bundle shown in Fig.6.

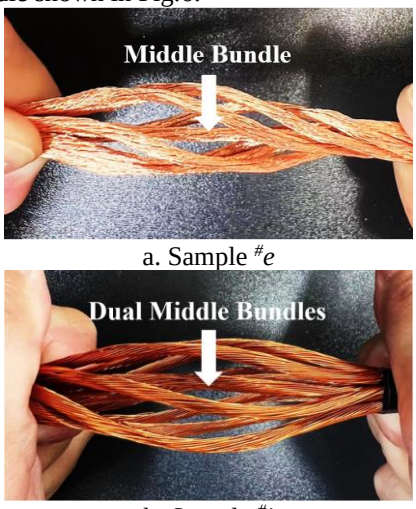

a. Sample #*e*

b. Sample #*i*

Fig. 6. Schematic diagram of middle bundles

Therefore, there are two kinds of bundles in litz wires,

middle bundles, and outer bundles respectively. To specify the twisting times and thus the required wire length for axial thermal conductivity calculation in section III, the middle and outer layers bundle are introduced in Fig.7.

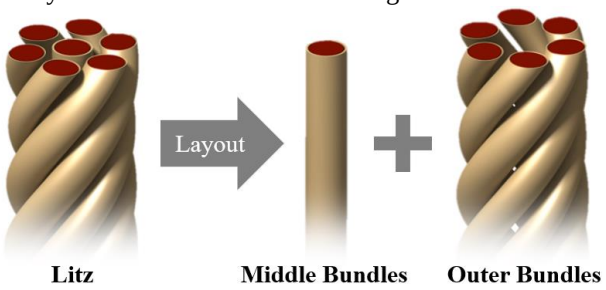

Fig. 7. Middle bundles and outer bundles

Depending on the conductors locations, two categories of 'middle bundles' and 'outer bundles' are defined in Fig. 8, with the ratio of 1:6 referring to samples #*a*, #*e*, and #*h*.

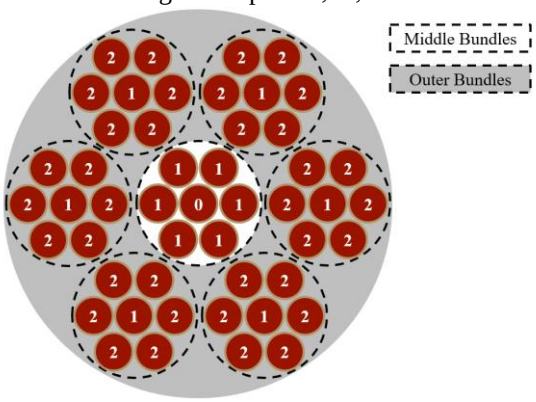

Fig. 8. Number of twisting times for each kind of conductors

Fig.8 also shows an example of the total twisting times for samples #*a*, #*e*, and #*h* with 1 middle bundle and 6 outer bundles. 0 refers to the untwisted conductors, 1 means that the wires have been twisted once and 2 refers to the case that enameled wires have been twisted twice. For samples #*b*, and #*d*, the structure with less than 6 bundles, they do not have a middle bundle, all the bundles are twisted at least once, as shown in the grey circle in Fig.8.

For the 9 samples in this paper, the middle bundles number is 0, 1, or 2. The bundles length can be further calculated respectively through the thread pitch. The total number of bundles in a litz wire, and the number of middle and outer bundles in each sample investigated in this paper are listed in TABLE III.

TABLE III
MIDDLE BUNDLES QUANTITY RELATIONSHIP

Samples	*Total number of bundles*	*Number of Middle Bundles* (n_M)	*Number of Outer Bundles* (n_O)
#*a*	7	1	6
#*b*	5	0	5
#*c*	6	1	5
#*d*	5	0	5
#*e*	7	1	6
#*f*	12	2	10
#*g*	10	2	8
#*h*	7	1	6
#*i*	10	2	8

In general, middle bundles number in litz wires is determined by the total number of bundles. For example, there are no middle bundles for litz wires with less than 6 bundles, and there is 1 middle bundle for litz wires with 6~7 bundles. There are 2 middle bundles for litz wires with more than 10 bundles.

II. CALCULATION TECHNIQUES

Based on the litz wire structure in section II, this section presents two methods to calculate the equivalent axial thermal conductivity of litz wire, (i) equivalent length model (ELM) and (ii) equivalent medium model (EMM). It is assumed with ELM that dominated heat transfer is along the enamel wires, i.e., path#1 in Fig.9 (a). For ELM, the enamel wires are assumed separated from each other. Whilst it is assumed with EMM that dominated heat transfer is along the litz wire axial direction, i.e., path#2 in Fig.9 (b). For EMM, litz wire is assumed a uniform mixture of copper and insulation materials. The heat is transferred from one end to another end of a mixture material cylinder with the same cross-section area of litz wire.

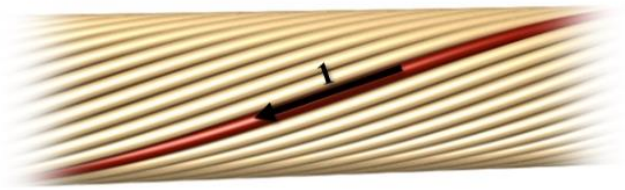

a. Dominated heat transfer direction is along the enamel wires

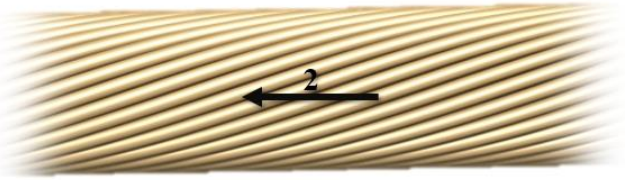

b. Dominated heat transfer direction is along the litz wire

Fig. 9. Two heat transfer paths

A. Equivalent Length Model

It is assumed with ELM that there is no heat transfer between different enameled wires in the xy direction. Thus, the litz wire length is a critical factor for the axial thermal conductivity calculation, which can be calculated based on the bundles descriptions in section II. Enameled wires of the same lengths are classified as one type, which are determined by the twisting times in Fig.8. The enamel wires length distribution in Fig.10, corresponds to the structure in Fig.8, i.e., 1 middle bundle and 6 outer bundles.

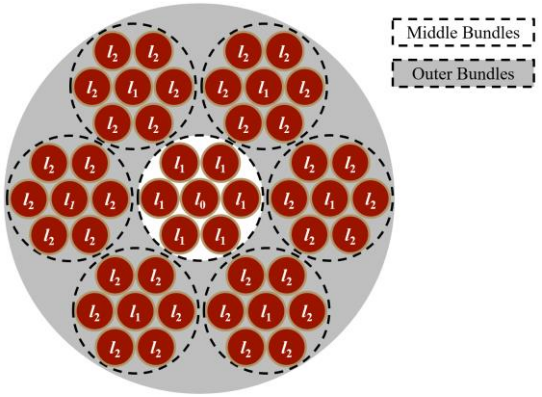

Fig. 10. The length distribution of the conductors in each litz wire

The lengths l_0, l_1 and l_2 in Fig.9 are calculated with (1), (2), and (3). l_0, l_1 and l_2 corresponds to the wire length that is untwisted, twisted once, and twisted twice, respectively.

$$l_0 = l_e \tag{1}$$

$$l_1 = {l_e}/{cos\,\alpha} \tag{2}$$

$$l_2 = {l_e}/{cos^2\,\alpha} \tag{3}$$

where, l_e is the length of litz wires. The three aforementioned types of enamel wires in Fig.10 and the thermal transfer through the varnish are in parallel as shown in Fig.11.

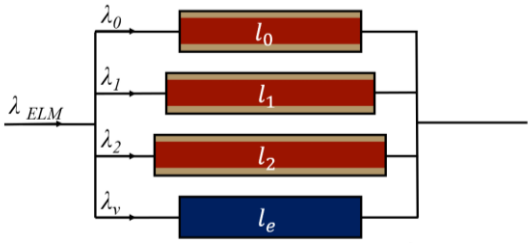

Fig. 11. Thermal conductivity in each kind of conductor length

In Fig.11, λ_{ELM} is the litz wires thermal conductivity calculated with ELM, λ_0, λ_1, λ_2 are the thermal conductivity of each kind of enamel wires corresponding to wires with length l_0 , l_1 , l_2 respectively, λ_V is the varnish thermal conductivity. Since the varnish process is conducted after litz wires are twisted, its length is equivalent to litz wire length l_e. λ_i in (4) is the transformed thermal conductivity based on copper and wires that corresponds to the various lengths in Fig.10, i=0, 1, 2,

$$\lambda_i = \frac{l_e}{l_i}\left(\frac{\lambda_{Cu} + \lambda_{En}((1+\sigma)^2 - 1)}{(1+\sigma)^2}\right) \tag{4}$$

where, λ_{Cu} and λ_{En} represent the thermal conductivity of the bare copper and enamel respectively, σ is the ratio of the enamel thickness to copper diameter, which is 0.05 in this paper. The calculation method of each kind of single enameled wire length and varnish is shown in (5).

$$\lambda_{ELM} = \frac{\lambda_0 A_0 + \lambda_1 A_1 + \lambda_2 A_2 + \lambda_V A_V}{A_e} \tag{5}$$

where, A_i is the sum cross-section area of the enamel wires in length l_i, A_V is the cross-section area of varnish, A_e is the cross-section area of the litz wire. A_i and A_V can be obtained with (6) and (7).

$$A_i = (1+\sigma)^2 \left(\frac{D_w}{2}\right)^2 \pi \cdot n_i \tag{6}$$

$$A_V = A_e - A_0 - A_1 - A_2 \tag{7}$$

where, D_w is the diameter of bare copper wires, n_i is the sum number of the enamel wires in length l_i, as for the structure of 1 middle bundle and 6 outer bundles in Fig.10, n_i can be obtained by the number of enamel wires N_M as follow.

$$n_0 = 1/49 N_M \tag{8}$$

$$n_1 = 12/49 N_M \tag{9}$$

$$n_2 = 36/49 N_M \tag{10}$$

A_e is the cross-section area of the litz wire. The λ_{ELM} is obtained as (11).

$$\lambda_{ELM} = \frac{\lambda_0 A_0 + \lambda_1 A_1 + \lambda_2 A_2 + \lambda_V A_V}{A_e}$$
$$= \frac{D_w^2 \pi}{4A_e} \cdot (\lambda_{Cu} + \lambda_{En}((1+\sigma)^2 - 1)) \frac{\sum_{i=0,1,2} \cdot n_i \cdot \cos^i \alpha}{(n_0 + n_1 + n_2)}$$
$$+ \lambda_V \left(1 - \frac{D_w^2 \pi (1+\sigma)^2 (n_0 + n_1 + n_2)}{4A_e}\right) \tag{11}$$

B. Equivalent Medium Model

With EMM, it is assumed there is heat transfer in the xy direction between different components, including copper, enamel, and varnish. In this case, the cross area in each bundle is different in Fig. 12, which illustrates the sample $^{\#}a$, $^{\#}e$, and $^{\#}h$, with 1 middle bundle and 6 outer bundles.

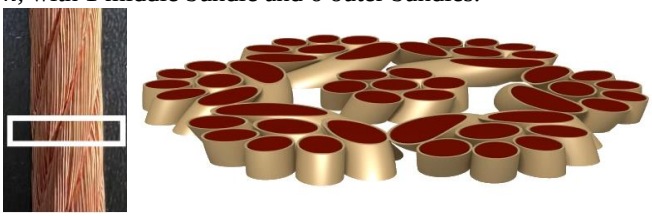

a. Sample $^{\#}h$ b. Differenrital length of a litz wire

Fig.12. Conductor distribution in differential length

The cross area for each component is calculated with twisting angles seen in Fig.13. Based on the twisting times in section IIB, twisting angles θ_0 , θ_1 , θ_2 , θ_3 , and θ_4 are calculated. θ_0 is close to 0° for the untwisted wires in (12). θ_1 is the enameled wires twisted once, which is close to the thread pitch $\boldsymbol{\alpha}$ in (13). θ_2 corresponds to the wires that are twisted twice in opposite directions, which thus is close to 0° in (14). θ_3 in (15) means the angle of the wires that is twisted twice in the same direction and is close to $2\boldsymbol{\alpha}$ in (15). θ_4 in (16) is twisted twice by two vectors at an angle of 60°, as shown in Fig.14. In Fig.14, vector 1 shows the direction that the enamel wires are twisted within bundles and vector 2 indicates that the bundles are twisted within the litz wire.

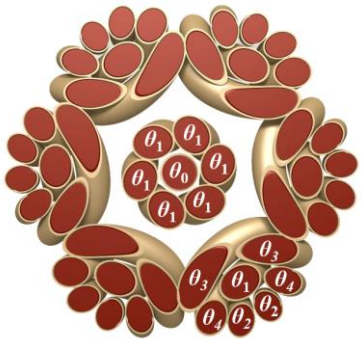

Fig. 13. The angle distribution of the enamel wires in each bundle

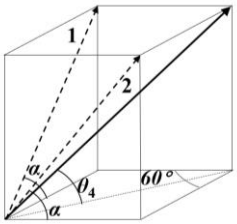

Fig. 14. Calculation method of θ_4

$$\theta_0 = 0 \quad (12)$$
$$\theta_1 = \alpha \quad (13)$$
$$\theta_2 = 0 \quad (14)$$
$$\theta_3 = 2\alpha \quad (15)$$
$$\theta_4 = \tan^{-1}(\frac{\sqrt{3}}{3}\tan\alpha) \quad (16)$$

With EMM, the length is same for all the components (copper, enamel, varnish), with different cross area as seen in Fig. 13 that can be calculated with the aforementioned twisting angles. Based on EMM idea, the thermal conductivity of the mixed material is similar to the volume ratio of the material in differential length as shown in Fig.15.

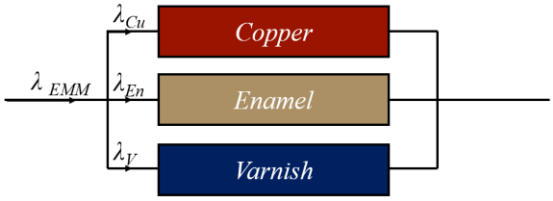

Fig. 15. Equivalent thermal conductivity in litz wires

The cross-section of enameled wires is similar to elliptical columns in a small section of litz wire in (17).

$$A_i = \pi ab = \frac{{D_w}^2\pi}{4\cos\theta_i} \quad (17)$$

where, A_i is the cross-sectional area for each ellipse in the enamel wires at angle θ_i, i=0, 1, 2, 3, 4. a and b represent the long and short radii of the ellipse. Set A'_{Cu}, A'_{En}, A'_V as the sum of cross-section area at θ_i, for bare copper, enamel, and varnish, respectively. The cross-section area of copper $A'_{Cu}$is calculated with (18):

$$A'_{Cu} = \sum_{i=0,1,2,3,4} \frac{n_i {D_w}^2\pi}{4\cos\theta_i} \quad (18)$$

where, n_i is the total number of the wires at the same angle, i=0, 1, 2, 3, 4. As for the structure of 1 middle bundle and 6 outer bundles in Fig.13, n_i can be obtained as follow.

$$n_0 = 1/49N_M \quad (19)$$
$$n_1 = 12/49N_M \quad (20)$$
$$n_2 = 12/49N_M \quad (21)$$
$$n_3 = 12/49N_M \quad (22)$$
$$n_4 = 12/49N_M \quad (23)$$

where, N_M is the total number of enamel wires. According to the properties of the enameled wires, the cross-section area of the enamel material A'_{En} is shown in (24)

$$A'_{En} = ((1+\sigma)^2 - 1)\,A'_{Cu} \quad (24)$$

where, σ is the ratio of the enamel thickness in each enamel wires to copper diameter, which is 0.05 in this case. The cross area of epoxy resin A'_V is:

$$A'_V = A_e - A'_{Cu} - A'_{En} \quad (25)$$

where, A_e is the total litz wire cross-section area. The litz wire equivalent thermal conductivity λ_{EMM} obtained with EMM is:

$$\lambda_{EMM} = \frac{\lambda_{Cu}A'_{Cu} + \lambda_{En}A'_{En} + \lambda_V A_V}{A_e}$$
$$= \frac{{D_w}^2\pi}{4A_e}(\lambda_{Cu} + \lambda_{En}((1+\sigma)^2 - 1))) \cdot \sum_{i=0,1,2,3,4} \frac{n_i}{\cos\theta_i}$$
$$+\lambda_V \cdot (1 - \frac{{D_w}^2\pi(1+\sigma)^2 \sum_{i=0,1,2,3,4} \frac{n_i}{\cos\theta_i}}{4\,A_e}) \quad (26)$$

III. Experiment Validation

A specially made test rig is used to test the 9 litz samples in section II to validate the proposed analytical methods in section III. The results calculated from the analytical methods and experimental testing are compared and analyzed.

A. Test Principle

A test rig in Fig.16 was designed to mearure the axial thermal conductivity of a litz wire. In Fig.16, A is a copper plate with heaters embeded, which temperature is controled with a constant heat source. Fixture B and D are used to hold the litz wire samples C. E is made of copper with cooling channls inside, which temperature can be controlled by the coolant flowing through the cooling channels. With the mearured temperature difference across the sample, temperatur differences at two ends of heat and cold plates, one can derive the aixial thermal conductivity of measured sample. Insulation brancket is applied to the samples and the test rig to stop the heat disspation from sample to enviroment.

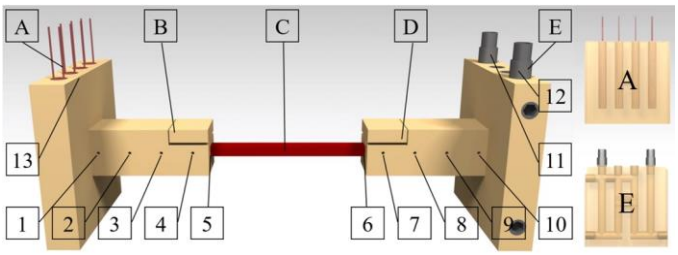

Fig. 16. Test rig

In Fig.16, points 1~13 are temperature measuring point. Temperature difference between points 1, 2, 3 can be used to

calculate the heat flux q_B flowing through B, while 8, 9, 10 can be used to calculate the heat flux q_D flowing through D. Temperature at piont 4 can be used to check the contact between the litz wire sample and B. Similarly, 7 is used to check the contact bewteen the D and litz wire samples.Temperature difference from points 5 and 6 is used to calculate axial thermal conductivity, using the calculated heat flux across litz wire samples C. 11, 12 corresponds to the coolant inlet and outlet temperature, respectively. 13 is used to measure the temperature of hot plate for the control of power supply

Under a thermally steady condition, the heat flux q_B flowing through B should be equal to q_D through D, which is same with that q_C through C (litz wire sample). Equations (27) and (28) can then be used to calculate the axial flux and the axial thermal conductivity of measured litz wire sample.

$$q_B = -\lambda_{Cu} A_B \frac{\Delta T_{1,3}}{\Delta x_{1,3}} \quad (27)$$

$$q_C = -\lambda_{Sample} A_C \frac{\Delta T_{5,6}}{\Delta x_{5,6}} \quad (28)$$

where A_B is the cross-section area of fixture B, A_C is the cross-section area of each test sample C. $\Delta T_{i,j}$ is the temperature difference between point i and point j, $\Delta x_{i,j}$ is the physical distance between point i and point j, λ_{Sample} is the thermal conductivity to be tested in each sample.

The test rig is shown in Fig.17, which is covered with thermal insulating asbestos (Calcium-Magnesium Silicate Thermal Insulating Sheet), and the outermost part is a foam box to ensure a good thermal insulation of the test rig to stop any heat dissipated from sample to enviroment.

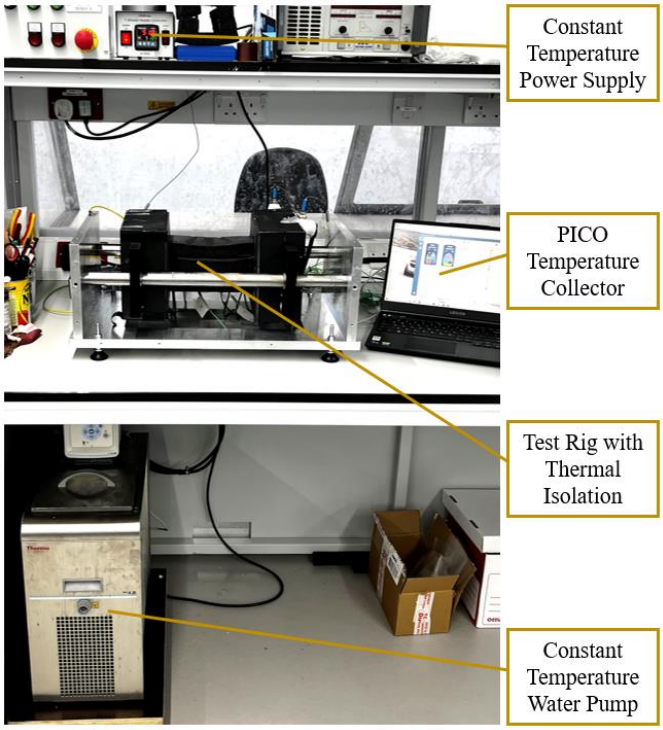

Fig.17. Practical experimental bench

In Fig.17, Constant Temperature Power Supply with PID controller is used as the heat source to heat the hot plate, which temperature is controlled at three different temperatures, i.e., 50℃, 70℃, and 90℃. PICO Collecter is used for temperature measurement. Constant Tempreture Water Pump supplys cooling water to the cold plate of test rig at 5°C to remove the heat transferred from hot plate to cold plate through the sample.

B. Calibration

As shown in Fig.17, the test rig has been thermally insulated with Calcium-Magnesium Silicate Thermal Insulating Sheet and foam box to minimize the losses that are dissipated to the environment. Furtherly, following procedures are conducted to ensure the testing accuracy with samples tested.

Three samples in Fig.18 whose cross-section areas and lengths are similar to litz wire samples in Fig. 3 are made from pure copper [HC101] with known thermal conductivity (391W/m·K), and three other samples are made from aluminum [HE30TF] (180W/m·K). With the same dimensions, the losses dissipated to the ambient will be same for the test and litz wire samples. These two types of material are chosen as their thermal conductivities falling in the range of litz wires axial thermal conductivities based on prediction of thermal models developed.

All the test samples in Fig.18 and litz wire samples are tested under the same conditions: high temperature end is approximate to 50℃, 70℃ and 90℃, respectively, while the low temperature end is approximate to 5℃. Utilizing formulas (27) and (28), the thermal conductivity of the litz wire samples can be obtained.

Fig. 18. Cu and Al calibration strip

During the validation process, multiple measurements in different length of strips are conducted to ensure the reliabilities and accuracies of measurements, one set of the test data is shown in Fig. 19 (a) and Fig.19 (b), all of the results are listed in Table IV. From the data shown in Table IV, one can see that the measured axial thermal conductivities are close to the samples and the measurement errors are within 1.15%. The same measurement techniques are then applied to the litz wire samples measurement to ensure the accuracy of the measurement of litz wires.

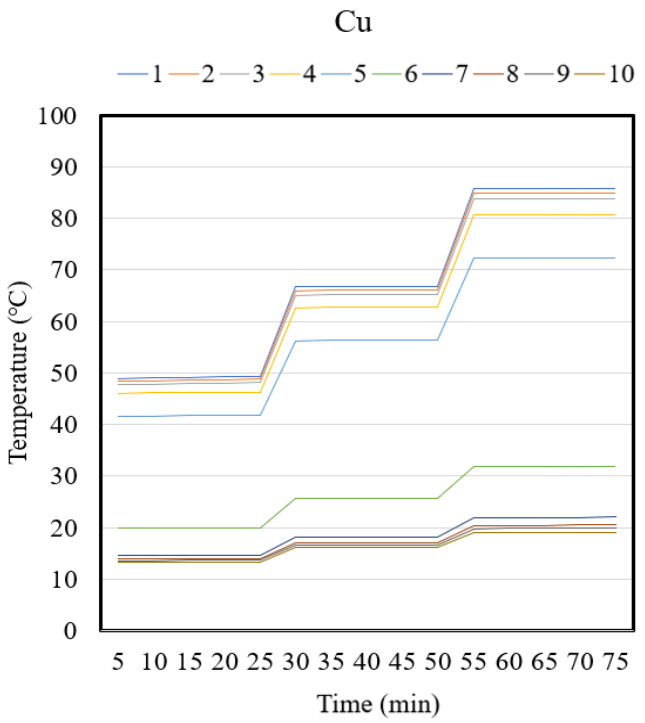

a. Copper strip in 100mm

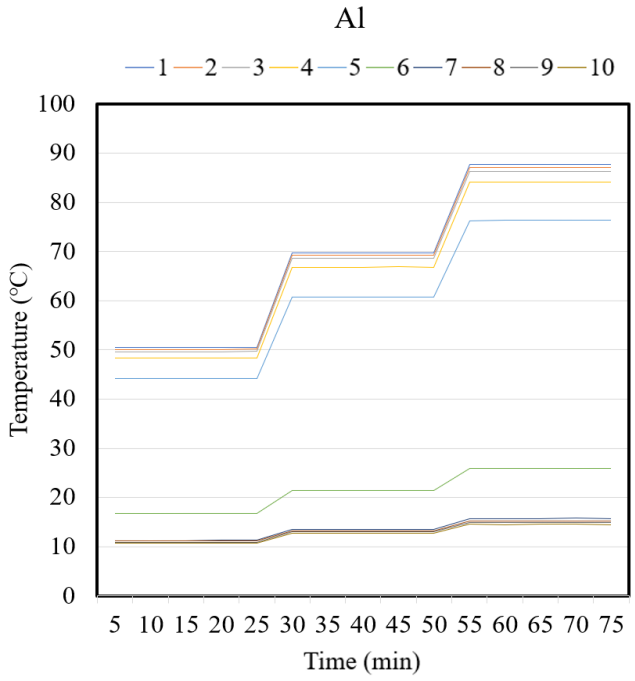

b. Aluminum strip in 100mm

Fig. 19. Testing results of two strips in 100mm

TABLE IV
THE TOLERANCE OF TEST BENCH

Strips	*Thermal Conductivity*	*Test Result*	*Error*
Cu [HC101] 100mm	391W/m·K	388.2 W/m·K	0.72%
Cu [HC101] 150mm	391W/m·K	387.8 W/m·K	0.82%
Cu [HC101] 200mm	391W/m·K	386.5 W/m·K	1.15%
Al [HE30TF] 100mm	180W/m·K	181.4 W/m·K	0.78%
Al [HE30TF] 150mm	180W/m·K	180.1 W/m·K	0.06%
Al [HE30TF] 200mm	180W/m·K	178.6 W/m·K	0.78%

C. Test data

The average measured data is used to calculate the samples axial thermal conductivity, using formulas (29) and (30). One set of three times test data for samples, such as $^{\#}a$, with varnish and without are shown in Fig. 20 (a) and Fig. 20 (b). Similarly, testing results are plotted for all other samples in 100mm (from $^{\#}b$ to $^{\#}i$) and put in the appendix.

$$\lambda_{Sample} = \frac{\Delta x_{5,6} \cdot (q_B + q_D)/2}{\Delta T_{5,6} \cdot A_C} \tag{29}$$

$$\lambda_{Sample} = \frac{\Delta x_{5,6} \cdot \lambda_{Cu} A_B (\Delta T_{1,3} + \Delta T_{8,10} + \delta_i)/(\Delta x_{1,3})}{2\Delta T_{5,6} \cdot A_C} \tag{30}$$

where δ_i is the correction coefficient of the measured temperature by thermocouples under i condition, which is obtained by placing the thermocouples together in a specific temperature hot bath.

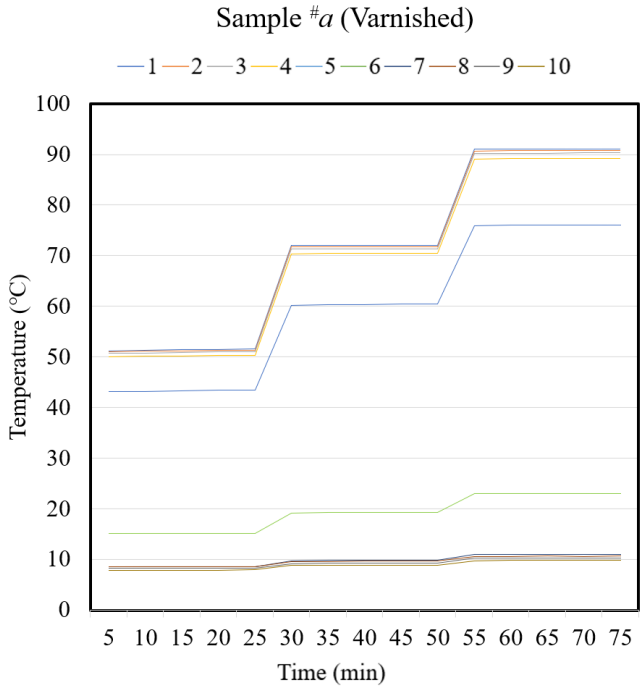

a. Sample $^{\#}a$ with varnished in 100mm.

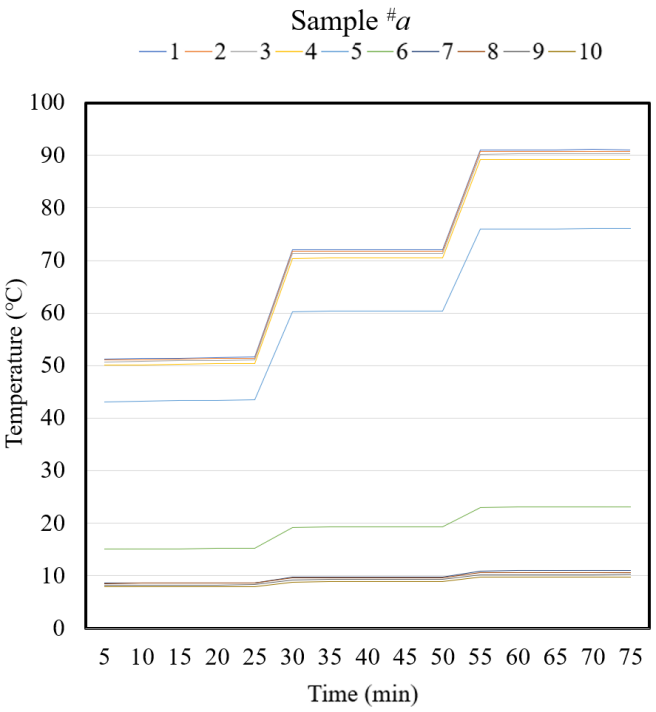

b. Sample #*a* without varnished in 100mm.

Fig. 20. Testing results of sample #*a*

The testing results for all the samples, as well as the calculated results using the analytical methods based on ELM and EMM, are listed in TABLE V, and plotted in Fig.21 for a clearer comparison.

TABLE V
COMPARISON OF TEST RESULTS OF THE 10 SAMPLES

Sample	*Average Test Result (w/m·°C)*	*Estimate Result*			
		λ_{ELM} *(w/m·°C)*	*Error 1*	λ_{EMM} *(w/m·°C)*	*Error 2*
#*a*	202.32	**195.19**	**3.52%**	241.24	19.24%
#*a*(V)	236.32	195.83	17.13%	**242.01**	**2.41%**
#*b*	212.30	**210.45**	**0.87%**	225.02	5.99%
#*c*	207.46	**205.98**	**0.71%**	242.00	16.65%
#*d*	277.15	**276.07**	**0.39%**	328.44	18.51%
#*d*(V)	280.89	**276.67**	**1.50%**	328.75	17.04%
#*e*	201.21	**189.55**	**5.79%**	242.37	20.46%
#*e*(V)	238.59	190.12	20.32%	**243.01**	**1.85%**
#*f*	208.18	**196.46**	**5.63%**	235.69	13.21%
#*f*(V)	232.31	196.98	15.21%	**236.20**	**1.67%**
#*g*	220.51	**201.85**	**8.46%**	249.17	13.00%
#*g*(V)	247.51	202.43	18.21%	**249.88**	**0.96%**
#*h*	228.96	**226.96**	**0.87%**	252.74	10.39%
#*i*	210.73	**206.72**	**1.90%**	243.01	15.32%

In TABLE V, Error 1 is the tolerances between the prediction result from ELM and the test result of the samples. Error 2 is the tolerances between the prediction result from EMM and the test result.

From TABLE V and Fig. 21, it can be noticed that ELM provides more accurate results compared to EMM for samples without varnish, while EMM is more suitable for samples with varnish. However, it should be noted that the thermal conductivity in both of the varnished and without varnished samples #*d* is closer to the results obtained with ELM. The

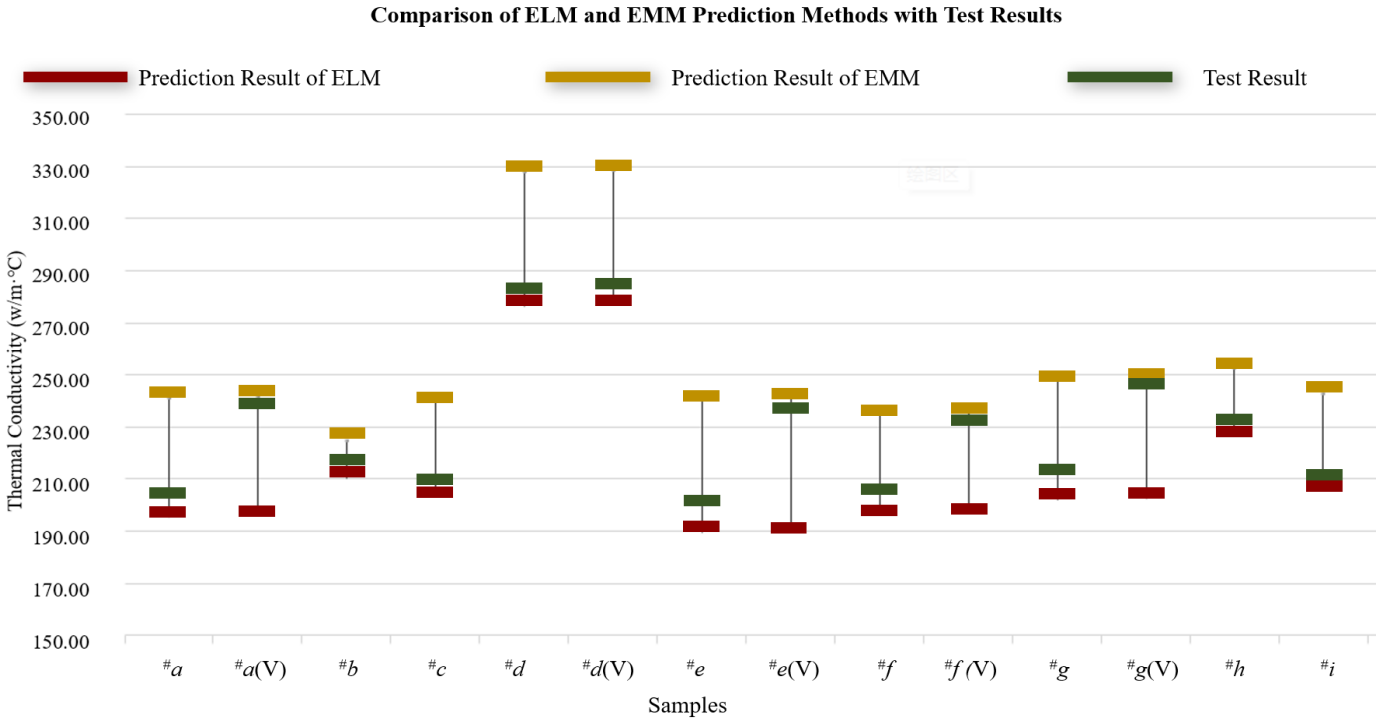

Fig. 21. Comparison of the results collected by the test rig, and the results predicted by ELM, and EMM

reason is the diameter of enameled wires is large and translate to a clear heat transfer path via copper.

It can be concluded that ELM can be used for any type litz wires without varnish process, transposition litz wire and round varnished litz wires, with less than 8.5% error. EMM is suitable for rectangular litz wires with varnish process, with less than 2.5% error.

Considering the litz wire shape and dimensions, quick formulas (31) and (32) are provided in this paper for litz wires based on ELM model and EMM, respectively.

Wrapped round litz wire:

$$\lambda_{ELM}(A_C, n_M, n_O, \alpha, N_w, D_w, \lambda_{Cu}) = \frac{\lambda_{Cu} l_e}{l_b} = \frac{\lambda_{Cu} {D_w}^2 \pi N_w (n_M \cos\alpha + n_O \cos^2\alpha)}{4(n_M + n_O) A_C} \quad (31)$$

Varnished rectangular litz wire:

$$\lambda_{EMM}(A_C, n_M, n_O, \alpha, N_w, D_w, \lambda_{Cu}) = \frac{\lambda_{Cu} A_{Cu}}{A_C} = \frac{\lambda_{Cu} {D_w}^2 \pi N_w (\frac{n_M}{\cos\alpha} + \frac{n_O}{\cos^2\alpha})}{4(n_M + n_O) A_C} \quad (32)$$

where, n_M is the number of middle bundles, n_O is the number of outer bundles in TABLE III and l_b is the bundles equivalent length. Litz wire axial thermal conductivity is mainly affected by the pitch angle, the distribution of bundles, the compress process, as well as the varnish process.

IV. Conclusion

Thermal model is critical to evaluate electrical machines thermal performance, which is important for next generation high power density electrical machines. Slot thermal conductivity is a complex but critical value in the process to build up 3D thermal models. The equivalent slot thermal conductivity in the axial direction is always ignored compared to that in the radial direction. However, the axial thermal conductivity is important to predict the thermal performance for electrical machines with enhanced cooling methods, where the heat is mostly dissipated to the ambient environment via the axial direction, such as end-winding sprayed cooling.

This paper proposes two models (ELM, and EMM) based on the twist angle, number of middle bundles, etc. to calculate litz wires axial thermal conductivity, which are more difficult compared to traditionally wound wires, due to the twisting characteristics. 9 litz samples are used as case studies in this paper covering various litz wire types, such as being varnished and without, rectangular or round, and different thread pitch. A specially designed and manufactured test rig is used to validate the models. It is concluded that ELM is more suitable for litz wires without varnish, round litz wires, and transposition litz wires, while EMM is more accurate to predict the thermal conductivity of varnished rectangular litz wires. Analytical formulas are also presented in this paper to provide guidelines for researchers in this field.

Appendix

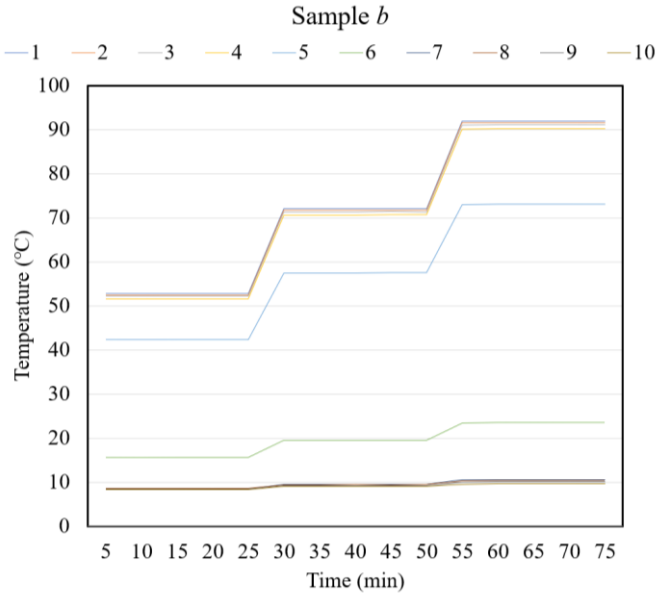

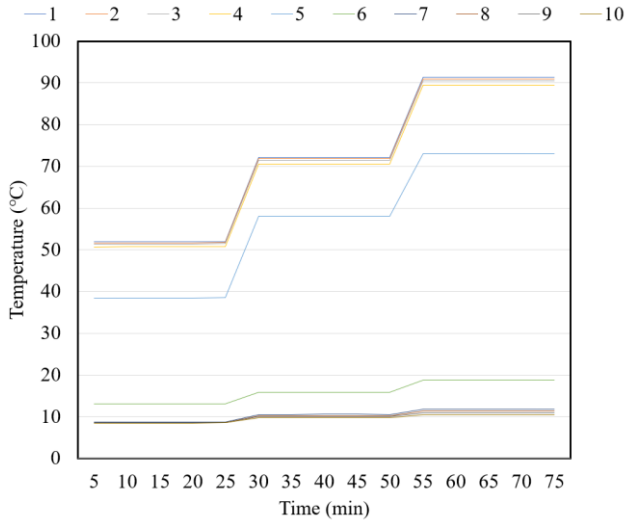

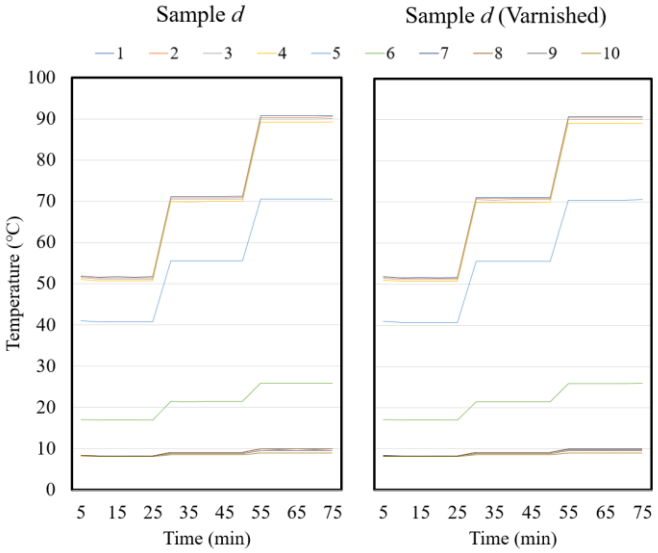

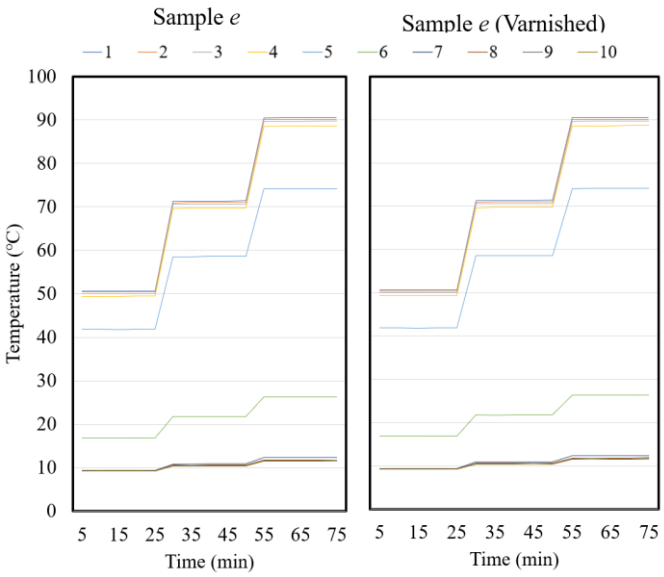

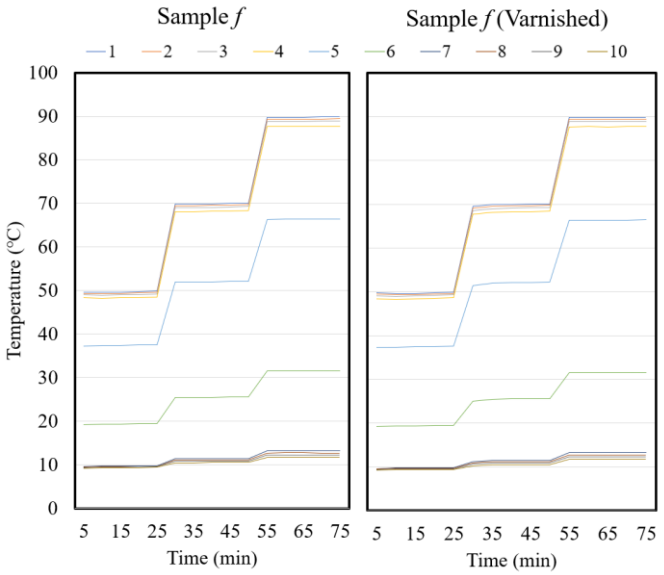

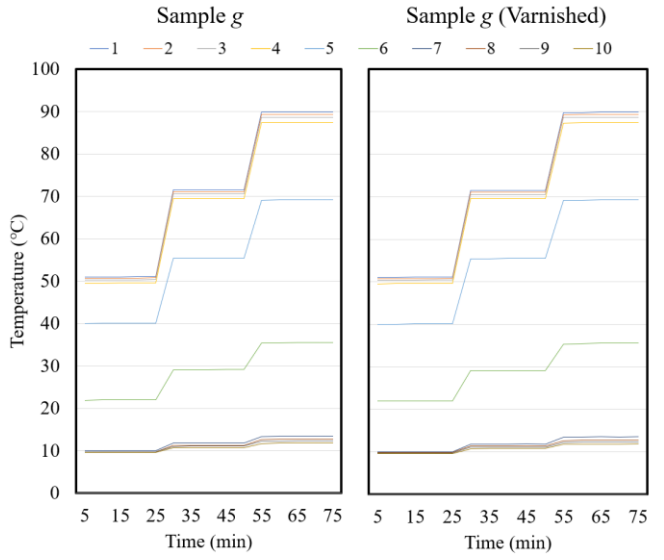

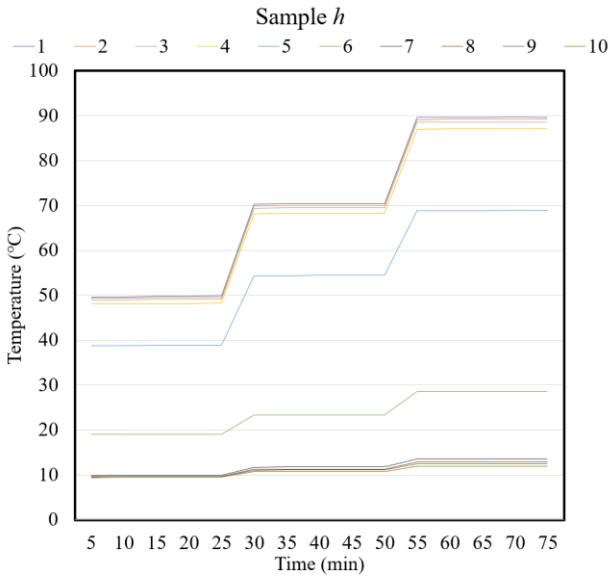

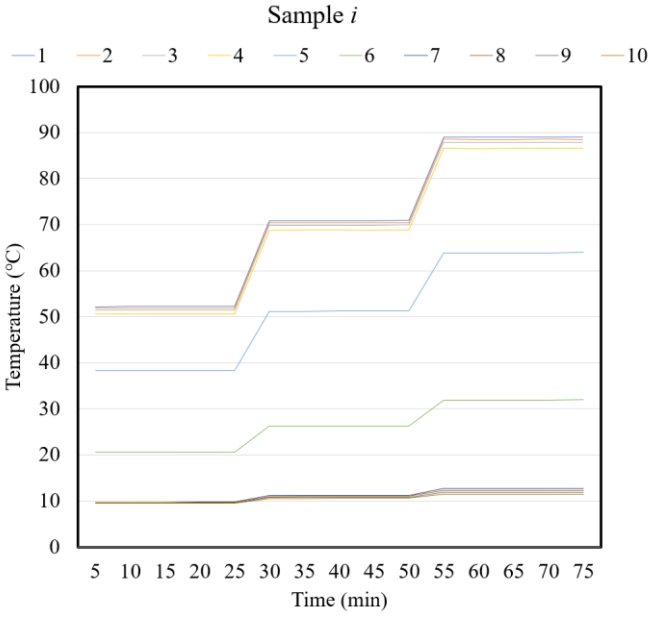

V. REFERENCE

[1]. D. Gerada, A. Mebarki, N. L. Brown, C. Gerada, A. Cavagnino and A. Boglietti, "High-Speed Electrical Machines: Technologies, Trends, and Developments," in IEEE Transactions on Industrial Electronics, vol. 61, no. 6, pp. 2946-2959, June 2014, doi: 10.1109/TIE.2013.2286777.

[2]. A. Bardalai, X. Zhang, T. Zou, D. Gerada, J. Li and C. Gerada, "Comparative Analysis of AC losses with round magnet wire and Litz wire winding of a High – Speed PM Machine," 2019 22nd International Conference on Electrical Machines and Systems (ICEMS), 2019, pp. 1-5, doi: 10.1109/ICEMS.2019.8922173.

[3]. Palmieri M., Cascella G. L., Cupertino F.; "Design Methodologies for the Output Power Maximization of Synchronous Reluctance Machines" IET Electric Power Applications Volume 13, Issue 8, 1 August 2019, Pages 1131-1140, DOI: 10.1049/iet-epa.2018.5801.

[4]. E. L. Barrios, A. Ursúa, L. Marroyo and P. Sanchis,

"Analytical Design Methodology for Litz-Wired High-Frequency Power Transformers," in IEEE Transactions on Industrial Electronics, vol. 62, no. 4, pp. 2103-2113, April 2015, doi: 10.1109/TIE.2014.2351786.

[5]. F. Zhang et al., "Back-Iron Extension Thermal Benefits for Electrical Machines With Concentrated Windings," in IEEE Transactions on Industrial Electronics, vol. 67, no. 3, pp. 1728-1738, March 2020, doi: 10.1109/TIE.2019.2903758.

[6]. R. Tavakoli, E. M. Dede, C. Chou and Z. Pantic, "Cost-Efficiency Optimization of Ground Assemblies for Dynamic Wireless Charging of Electric Vehicles," in IEEE Transactions on Transportation Electrification, vol. 8, no. 1, pp. 734-751, March 2022, doi: 10.1109/TTE.2021.3105573.

[7]. X. Liu, D. Gerada, Z. Xu, M. Corfield, C. Gerada and H. Yu, "Effective Thermal Conductivity Calculation and Measurement of Litz Wire Based on the Porous Metal Materials Structure," in IEEE Transactions on Industrial Electronics, vol. 67, no. 4, pp. 2667-2677, April 2020, doi: 10.1109/TIE.2019.2910031.

[8]. A. A. Woodworth et al., "Thermal Analysis of Potted Litz Wire for High-Power-Density Aerospace Electric Machines," 2019 AIAA/IEEE Electric Aircraft Technologies Symposium (EATS), 2019, pp. 1-13, doi: 10.2514/6.2019-4509.

[9]. H. P. Liu and J. J. Hahne, "High-speed compulsator stator thermal management," in IEEE Transactions on Magnetics, vol. 39, no. 1, pp. 357-361, Jan. 2003, doi: 10.1109/TMAG.2002.806414.

[10]. T. Balachandran, S. Lin, C. Ward and K. S. Haran, "Improving the Thermal Conductivity of Form-Wound Litz-Wire Windings for Slot-less Machines," 2021 IEEE International Electric Machines & Drives Conference (IEMDC), 2021, pp. 1-8, doi: 10.1109/IEMDC47953.2021.9449567.

[11]. C. Liu et al., "Experimental Investigation on Oil Spray Cooling with Hairpin Windings," in IEEE Transactions on Industrial Electronics, vol. 67, no. 9, pp. 7343-7353, Sept. 2020, doi: 10.1109/TIE.2019.2942563.

[12]. F. Zhang et al., "Electrical Machine Slot Thermal Condition Effects on Back-Iron Extension Thermal Benefits," in IEEE Transactions on Transportation Electrification, vol. 7, no. 4, pp. 2927-2938, Dec. 2021, doi: 10.1109/TTE.2021.3085822

[13]. R. Burke, A. Giedymin, Z. Wu, H. Chuan, N. Bourne and J. G. Hawley, "A Lumped Parameter Thermal Model for Single-Sided AFPM Machines With Experimental Validation," in IEEE Transactions on Transportation Electrification, vol. 6, no. 3, pp. 1065-1083, Sept. 2020, doi: 10.1109/TTE.2020.2998110.

[14]. X. Yi, T. Yang, J. Xiao, N. Miljkovic, W. P. King and K. S. Haran, "Equivalent Thermal Conductivity Prediction of Form-Wound Windings with Litz Wire Including Transposition Effects," in IEEE Transactions on Industry Applications, vol. 57, no. 2, pp. 1440-1449, March-April 2021, doi: 10.1109/TIA.2021.3053500.

[15]. N. Simpson, R. Wrobel and P. H. Mellor, "Estimation of Equivalent Thermal Parameters of Impregnated Electrical Windings," in IEEE Transactions on Industry Applications, vol. 49, no. 6, pp. 2505-2515, Nov.-Dec. 2013, doi: 10.1109/TIA.2013.2263271.

[16]. M. Delhommais, J. Schanen, F. Wurtz, C. Rigaud, S. Chardon and S. Vighetti, "Thermal model of Litz wire toroidal inductor based on experimental measurements," 2018 IEEE Applied Power Electronics Conference and Exposition (APEC), 2018, pp. 2658-2665, doi: 10.1109/APEC.2018.8341392.

[17]. G. Salinas, A. Delgado, J. A. Oliver and R. Prieto, "Fast FEA Thermal Simulation of Magnetic Components by Winding Equivalent Layers," 2018 IEEE Energy Conversion Congress and Exposition (ECCE), 2018, pp. 7380-7385, doi: 10.1109/ECCE.2018.8557714.

[18]. A. Delgado, G. Salinas, J. Rodríguez, J. A. Oliver and J. A. Cobos, "Finite Element Modelling of Litz Wire Conductors and Compound Magnetic Materials based on Magnetic Nano-particles by means of Equivalent Homogeneous Materials for Wireless Power Transfer System," 2018 IEEE 19th Workshop on Control and Modeling for Power Electronics (COMPEL), 2018, pp. 1-5, doi: 10.1109/COMPEL.2018.8460012.

[19]. Q. Deng et al., "Frequency-Dependent Resistance of Litz-Wire Square Solenoid Coils and Quality Factor Optimization for Wireless Power Transfer," in IEEE Transactions on Industrial Electronics, vol. 63, no. 5, pp. 2825-2837, May 2016, doi: 10.1109/TIE.2016.2518126.

[20]. M. Jaritz, A. Hillers and J. Biela, "General Analytical Model for the Thermal Resistance of Windings Made of Solid or Litz Wire," in IEEE Transactions on Power Electronics, vol. 34, no. 1, pp. 668-684, Jan. 2019, doi: 10.1109/TPEL.2018.2817126.

[21]. A. Bardalai et al., "Reduction of Winding AC Losses by Accurate Conductor Placement in High Frequency Electrical Machines," in IEEE Transactions on Industry Applications, vol. 56, no. 1, pp. 183-193, Jan.-Feb. 2020, doi: 10.1109/TIA.2019.2947552.

[22]. R. Wrobel, S. Ayat and J. L. Baker, "Analytical methods for estimating equivalent thermal conductivity in impregnated electrical windings formed using Litz wire," 2017 IEEE International Electric Machines and Drives Conference (IEMDC), 2017, pp. 1-8, doi: 10.1109/IEMDC.2017.8002003.

[23]. S. Nategh, S. Øvrebø, S. Mahdavi and O. Wallmark, "Thermal modeling of a permanent magnet machine built using Litz wire," 2015 International Conference on Electrical Systems for Aircraft, Railway, Ship Propulsion and Road Vehicles (ESARS), 2015, pp. 1-6, doi: 10.1109/ESARS.2015.7101462.

[24]. P. A. Kyaw, M. Delhommais, J. Qiu, C. R. Sullivan, J. Schanen and C. Rigaud, "Thermal Modeling of Inductor and Transformer Windings Including Litz Wire," in IEEE Transactions on Power Electronics, vol. 35, no. 1, pp. 867-881, Jan. 2020, doi: 10.1109/TPEL.2019.2914661.

[25]. J. Lyu, H. C. Chen, Y. Zhang, Y. Du and Q. S. Cheng, "Litz Wire and Uninsulated Twisted Wire Assessment Using a Multilevel PEEC Method," in IEEE Transactions on Power Electronics, vol. 37, no. 2, pp. 2372-2381, Feb. 2022, doi: 10.1109/TPEL.2021.3103867.